Energy & Environmental Science

PAPER

View Article Online
View Journal

Cite this: DOI: 10.1039/c4ee01034e

Performance of a mixing entropy battery alternately flushed with wastewater effluent and seawater for recovery of salinity-gradient energy†

Meng Ye,[ad] Mauro Pasta,[b] Xing Xie,[a] Yi Cui*[bc] and Craig S. Criddle*[ad]

Received 1st April 2014
Accepted 10th April 2014

DOI: 10.1039/c4ee01034e

www.rsc.org/ees

Salinity-gradient energy, also referred to as *blue energy*, is a largely untapped source of renewable energy. Coastal wastewater treatment plants discharge a continuous stream of low salinity effluent to the ocean and are thus attractive locations for recovery of blue energy. One method of tapping this gradient is a "*mixing entropy battery*" (MEB), a battery equipped with anionic and cationic electrodes that charges when flushed with freshwater and discharges when flushed with seawater. We constructed a plate-shape MEB, where the anionic electrode was Ag/AgCl, and the cationic electrode was $Na_4Mn_9O_{18}$ (NMO). Over a single cycle with a single cell, the net energy recovery was 0.11 kW h per m^3 of wastewater effluent. When twelve cells were connected in series, the net energy recovery (energy produced after subtracting energy invested) was 0.44 kW h per m^3 of wastewater effluent. This is 68% of the theoretical recoverable energy of 0.65 kW h per m^3 of wastewater effluent. We conclude that (1) wastewater effluent can be effectively used for charging of a MEB, (2) cells in series are needed to optimize net energy recovery efficiency, (3) there is a trade-off between net energy recovery efficiency and capital investment, (4) there is a trade-off between net energy recovery efficiency and power output, and (5) new electrode materials are needed to increase capacity, decrease cost, and to avoid release of Ag to seawater.

Broader context

Salinity-gradient energy, or blue energy, is present when low-salinity water (such as river water, lake water, treated domestic wastewater) mixes with saline water (such as seawater, brackish ground water, and brine). We investigated the potential use of a mixing entropy battery (MEB) at coastal wastewater treatment plants. The energy theoretically available for recovery is 0.65 kW h per m^3 of wastewater effluent, a value comparable to the current electrical demand of wastewater treatment plants. Using a plate-shape MEB to reduce internal resistance and increase efficiency, we achieved a net energy recovery efficiency of 68% from the mixing of domestic wastewater effluent and seawater.

Introduction

Current wastewater treatment is energy-intensive. Treatment of the 126 million cubic meters of domestic wastewater generated each day in the United States accounts for ~3% of the nation's electrical energy load.[1] Similar values are reported for other developed countries.[1] But this should not be the case: the theoretical chemical energy recoverable from organic matter and ammonium in the wastewater is ~1.5–2 kW h per m^3, about three times the electrical energy required for the treatment (~0.6 kW h per m^3) (ref. 2). Moreover, at many treatment plants, an untapped supply is the entropic energy available when low salinity wastewater effluent discharges to a saline water body. Theoretical calculations indicate that 0.65 kW h per of energy can be recovered from mixing of 1 m^3 of wastewater effluent with seawater, an amount comparable to the electrical energy currently consumed at wastewater treatment plants.[1] Globally, the potentially recoverable power at coastal treatment plants is estimated to be 18 GW (ref. 3). If the chemical and entropic energies are both recovered, wastewater treatment plants can become net power producers rather than consumers.

Others have investigated technologies for recovery of the entropic energy of mixing, often referred to as "blue energy".[4] Pressure retarded osmosis (PRO) and reverse electrodialysis (RED) have received the most attention.[5–13] The main drawback of these technologies is their use of membranes that are costly and prone to bio-fouling and mechanical rupture.[3] To address these issues, researchers developed membrane-less

[a]Department of Civil and Environmental Engineering, Stanford University, Stanford, California 94305, USA. E-mail: ccriddle@stanford.edu

[b]Department of Materials Science and Engineering, Stanford University, Stanford, California 94305, USA. E-mail: yicui@stanford.edu

[c]Stanford Institute for Materials and Energy Sciences, SLAC National Accelerator Laboratory, Menlo Park, California 94025, USA

[d]Woods Institute for the Environment and the Department of Civil and Environmental Engineering, Stanford University, Stanford, California 94305, USA

† Electronic supplementary information (ESI) available. See DOI: 10.1039/c4ee01034e

technologies, such as vapor compression[14] and hydrocratic generator.[15] These devices also have limitations: vapor compression and hydrocratic generators are mechanically complex. Recently, a new series of techniques has been invented, called "capacitive mixing", for blue energy recovery.[16–18] Three different types of "capacitive mixing" processes have been studied, including capacitive double layer expansion (CDLE) devices,[19] which store ions in the electric double-layer on the porous electrode surface when an external voltage is applied,[19,20] devices based on capacitive Donnan potential (CDP),[21–23] which employ ion-selective membranes to separate cations and anions, and mixing entropy batteries (MEBs),[24] which use battery electrodes that store and release specific ions. All processes involve a four-step cycle to extract energy from salinity gradients. An optimal cycle, in analogy to the Carnot cycle, is proposed to maximize energy recovery for these four-step cycles.[25] Each technique has a reverse process for desalination: capacitive deionization (CDI) is the reverse of CDLE;[26,27] membrane capacitive deionization (MCDI) is the reverse of CDP;[28–30] and a desalination battery reverses the process used in a MEB.[24,31] The MEB is a promising technology because it uses battery electrodes with relatively high specific capacity and low self-discharge. In the proof-of-concept study,[24] a high efficiency of energy extraction (74%) was inferred based on overpotentials with a single pair of electrodes. Net energy recovery efficiency was not directly measured, and operational factors affecting efficiency were not explored. We evaluated the potential of MEBs for recovery of blue energy from lake water and seawater salt gradients.[24] This study also entailed use of $Na_2Mn_5O_{10}$ and commercially available silver nanoparticles as the cationic and anionic electrodes. In this study, we evaluate the potential for recovery of blue energy at coastal wastewater treatment plants. We test treated wastewater effluent and seawater and change the cationic electrode material to a higher capacity material – $Na_4Mn_9O_{18}$ (NMO) (compared with $Na_2Mn_5O_{10}$ used in our previous work[24,31]). We investigate the potentials and limitations of these materials for this application. More importantly, we seek to identify process design trade-offs that must be considered regardless of the electrode materials used.

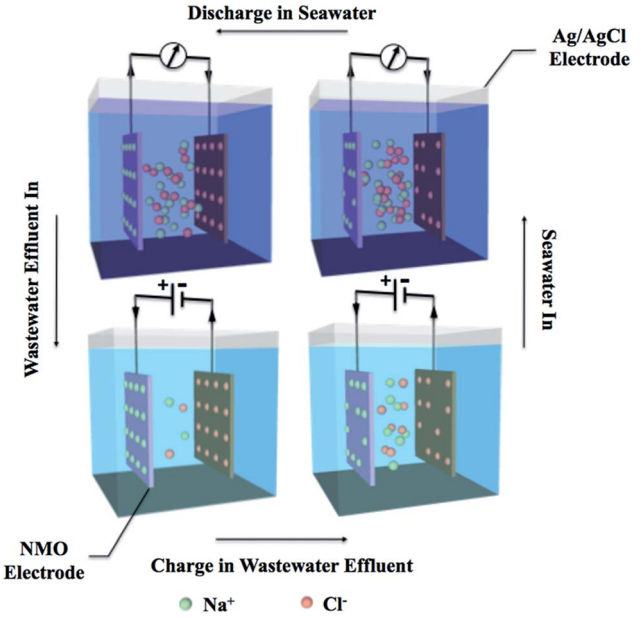

Fig. 1 Work cycle for a mixing entropy battery. In the bottom half of the figure, wastewater effluent flushes the cell and a current is applied (current direction is right to left) in order to charge the battery. Ions in the electrodes are released into solution. In the top half of the figure, seawater flushes the cell and energy is recovered (current direction is left to right) as the battery discharges. Ions in the seawater enter the electrodes. For the charge step, the cationic electrode half reaction is: $10Na_4Mn_9O_{18} \rightarrow 18Na_2Mn_5O_{10} + 4Na^+ + 4e^-$; the anionic electrode half reaction is: $4AgCl + 4e^- \rightarrow 4Ag + 4Cl^-$. For the discharge step, these reactions run in reverse.

Results and discussion

Fig. 1 illustrates the four-step cycle of the MEB first demonstrated in a previous proof-of-concept study.[24] In the presence of low salinity wastewater effluent, power is supplied at a constant current, releasing Na^+ from the cationic electrode and Cl^- from the anionic electrode. During this charge step, the reactions are:

Cationic electrode:

$$10Na_4Mn_9O_{18} \rightarrow 18Na_2Mn_5O_{10} + 4Na^+ + 4e^-$$

Anionic electrode:

$$4AgCl + 4e^- \rightarrow 4Ag + 4Cl^-$$

When this solution is replaced by seawater, the voltage between the electrodes increases due to the increase in NaCl concentration, current reverses direction, and power is generated as Na^+ and Cl^- ions are reincorporated into the electrodes. During this discharge step, the net reactions are:

Cationic electrode:

$$18Na_2Mn_5O_{10} + 4Na^+ + 4e^- \rightarrow 10Na_4Mn_9O_{18}$$

Anionic electrode:

$$4Ag + 4Cl^- \rightarrow 4AgCl + 4e^-$$

The net energy produced in each cycle is the path integral of the potential *vs.* charge curve. Energy out exceeds energy in because the battery is charged at a lower voltage (in wastewater effluent) and discharged at a higher voltage (in seawater). This process is made possible because charge and discharge occur at different NaCl concentrations. The additional energy is generated through the mixing of dilute wastewater effluent and seawater.

For these experiments, we used wastewater effluent from the Palo Alto Regional Water Quality Control Plant. The NaCl concentration of this solution is 0.032 M, a concentration that is a little higher than that of a typical river or lake. Seawater with a NaCl concentration of 0.6 M was obtained at Half Moon Bay, CA. Water samples were collected in plastic bottles, sealed, and stored at 4 °C. Initial battery voltages were reproducible, indicating stable ionic strength for all experiments. Both the

wastewater effluent and seawater were used directly without pretreatment. Details of the processes used to synthesize electrodes are described in the ESI.† The electrodes were pre-cycled (Fig. S2 and S3†) and then installed parallel to one another at a 1.7 mm distance in a 1.5 mL plate-shape cell. The internal resistance of the device was measured by potentiostatic impedance spectroscopy. Because the distance between electrodes was small, internal resistance was low: 17 Ω for wastewater effluent and 3 Ω for seawater.

The theoretically extractable blue energy was:[13]

$$\Delta G_{mix} = 2RT\left[V_E C_E \ln\frac{C_E}{C_M} + V_S C_S \ln\frac{C_S}{C_M}\right]$$

where C_E is the NaCl concentration in the wastewater effluent, C_S the NaCl concentration in seawater, V_E the volume of wastewater effluent, V_S the volume of seawater, R the universal gas constant, and T the absolute temperature. C_M is the NaCl concentration after complete mixing of wastewater effluent and seawater:

$$C_M = \frac{V_E C_E + V_S C_S}{V_E + V_S}$$

This is an approximation because activity coefficients are assumed equal to unity, and the entropy increase of water is neglected. When these factors are considered, they counterbalance one another.[13] Because wastewater effluent is the limiting resource, the key performance metric is energy production per unit volume of effluent. When $V_S \gg V_E$ (*i.e.* wastewater effluent is mixed with an infinite volume of seawater), $\Delta G_{mix}/V_E$ approaches 0.65 kW h per m^3 of wastewater effluent, the theoretically extractable free energy (ESI†).

In order to simulate cells in series, we recycled wastewater effluent (1.5 mL) back to a single cell, and applied a current to charge the cell. After completing this charge step, we removed the wastewater effluent, and reused it on the charge step in the next cycle. In the discharge step for every cycle, we flushed the cell with seawater. By repeating this cycle 12 times, we simulated 12 cells in series. The wastewater effluent became progressively more saline with each successive cycle. The current applied in the charge step of each cycle was 0.25 mA. The discharge current was also 0.25 mA, but in the reverse direction. The time for charge and discharge was 6 hours, giving a total cycle time of 12 hours. The HRT of wastewater effluent was 72 hours through 12 cycles. This HRT can be decreased by increasing the surface area of electrode exposed to flow or by increasing current density. We limited the number of cycles to 12 because the energy loss in the thirteenth cycle exceeded the energy available from the salinity gradient. The volume of seawater added to reach this point was 12 times the volume of the original wastewater effluent.

To assess voltage losses, we define a "voltage ratio" as the observed voltage rise when seawater (0.6 M) displaces freshwater (0.032 M) divided by the theoretical voltage rise calculated from the known salinity gradient (expressed as a percentage). We used the Nernst equation to calculate the theoretical voltage rise (ranges from 0.11 to 0.15 V depending upon cycle time) from the known concentration of NaCl in seawater and the calculated salt concentration in salinated wastewater effluent after charging (see ESI† for detailed calculation). We calculate the salt concentration after charging as the concentration of the wastewater effluent prior to charging (0.032 M) plus the increase in concentration from added charge (current times time). As shown in Fig. 2A, the voltage ratio decreased from 87% in the first cell to 64% in the final cycle. This is because the theoretical voltage rise decreases as the salinity gradient decreases. After the sixth cycle, voltage ratio stabilized: the decrease in voltage loss due to increased electrolyte salinity (and therefore conductivity) compensated for a decrease in the salinity gradient. Fig. 2B shows the net energy production and net power output per unit area of electrode per cycle. When the salinity gradient is high, the net energy recovered from the first cycle was 0.11 kW h per m^3 of wastewater effluent, about 17% of the theoretically available energy. Net energy recovery from the final cycle was only 0.01 kW h per m^3 of wastewater effluent. The decrease in the salinity gradient allowed little energy recovery despite a voltage ratio of 64%. Net power output per unit area of electrode per cycle decreased from 10.4 to 0.6 mW m^{-2}.

Fig. 2C illustrates the cumulative energy production and the overall energy efficiency for 12 cycles. Cumulative energy production is the sum of energy recoveries for individual cycles. Overall energy efficiency is cumulative energy production divided by the theoretical free energy of 0.65 kW h per m^3 of wastewater effluent. Cumulative energy production was 0.44 kW h per m^3 of wastewater effluent, and the overall energy efficiency was 68%. Theoretically, reuse of a given volume of wastewater effluent in an infinite number of cycles would maximize energy production per unit volume of wastewater effluent. However, there is a trade-off between net energy recovery and average power output. As the number of cycles increases, net energy recovery efficiency increases but average power output

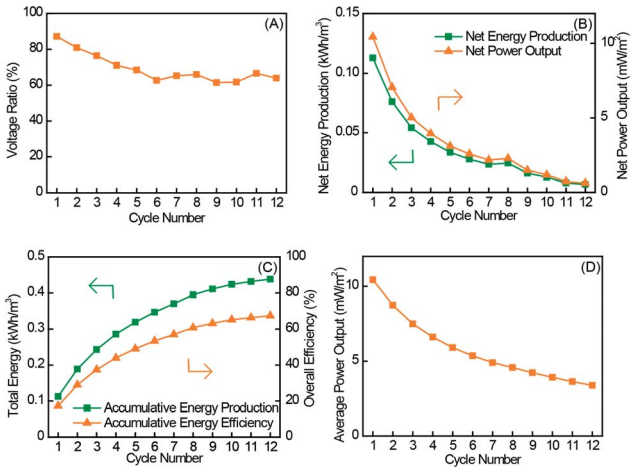

Fig. 2 Energy extraction from 12 mixing entropy battery cycles using recycled wastewater effluent. (A) Voltage ratio for each cycle through the series of cycles. (B) Net energy production and net power output from each cycle through the series of cells. (C) Total energy production and overall energy efficiency through the series of cells. (D) Average power output with different number of cycles.

decreases (Fig. 2D). Moreover, in real world applications, use of more cycles results in a higher capital cost because more electrode surface area is needed and/or more energy is invested for recycling of wastewater effluent. As shown in Fig. 2C, an efficiency of 60% can be achieved with 8 cycles in series. Increasing the number of cycles from 8 to 12 increases the energy efficiency by just 8%. These trade-offs are clearly important for future economic analyses.

In order to optimize the energy recovery by MEBs, we investigated several operational parameters. The first was the charge exchanged during the charge and discharge steps. The experiments were conducted by varying the cycle time from 40 minutes to 12 hours at a current of 0.25 mA. The path integral of the potential *vs.* charge curve indicates the net energy production from each cycle (Fig. 3A). More energy is extracted from a cycle when more charge is exchanged by extending the cycle time. Fig. 3B and S8† (plot the observed voltage rise verses theoretical voltage rise) illustrate the theoretical voltage rise, overpotential, and observed voltage rise as a function of cycle time. The theoretical voltage rise decreases from 0.15 to 0.11 V with cycle time. As cycle time increases, more electron equivalents are exchanged. This is because the current is constant ($Q_{\text{transferred}}$ = current × t_{cycle}). Exchange of more electron equivalents drives exchange of ions from the electrodes into solution. Exchange of more ions results in a lower voltage rise as cycle time increases, decreasing the gradient for energy recovery. As shown in Fig. 3B and S8,† the theoretical voltage rise is close to the observed voltage rise, reflecting a low and stable overpotential. High and stable voltage ratio (91% to 88%) was observed (Fig. S6†). Fig. 3C shows increasing energy production per cycle with increased cycle time. Energy production increased approximately linearly from 0.01 kW h per m^3 of wastewater effluent to 0.10 kW h per m^3 of wastewater effluent with increased cycle time (*i.e.*, charge exchanged). Ultimately, specific capacity of the electrode material becomes a limiting factor. Substantial energy loss resulted when the cycle time increased to 20 hours, and the charge curve crossed the discharge curve (Fig. S4†). The cycle time is thus limited by the capacity of the cationic electrode material (details in ESI†). Because only a portion of the capacity of the material can be used, more cells and material are required to achieve efficient energy recovery. Materials with higher specific capacity are desirable.

Another parameter that affects MEB performance is the current applied during the charge and discharge steps. To evaluate this variable, we fixed the total amount of charge at 1.5 mAh and evaluated 8 different currents ranging from 0.125 mA to 1 mA. As we increased the current applied, the quadrangle defined by the path integral of each charge–discharge cycle shrank along the *Y*-axis (Fig. 4A). This indicates a decrease in net energy production. Fig. 4B illustrates the voltage profiles for each cycle at different applied currents. The theoretical voltage rise did not change because the number of charges exchanged was fixed. Concentration differences between salinated wastewater effluent and seawater were the same for all cases. On the other hand, the overpotential increased almost linearly with current, resulting in a decrease in the observed

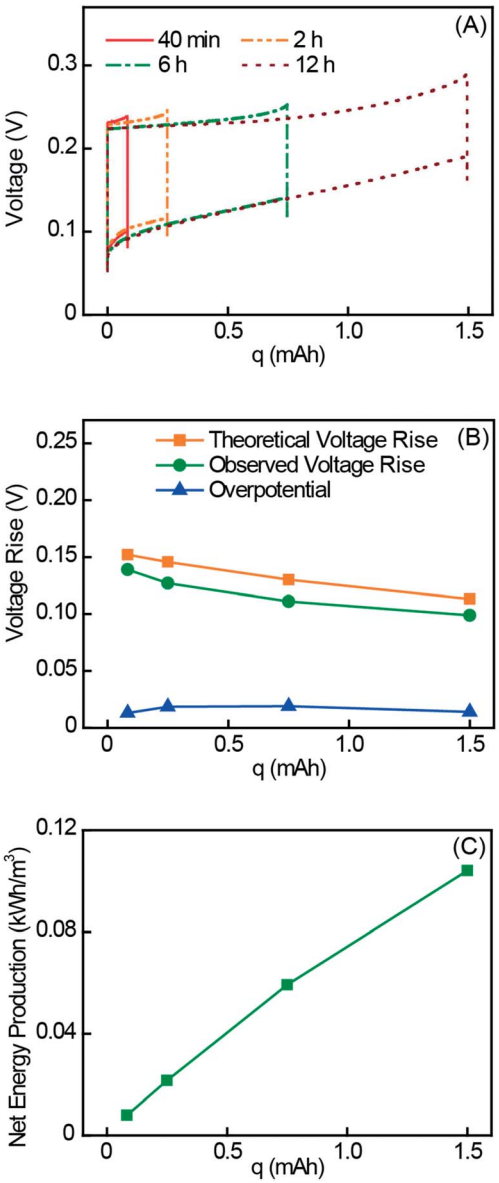

Fig. 3 Cycles with different amount of charges exchanged at a current of 0.25 mA. (A) Plot of voltage *vs.* charge showing energy extraction at cycle times of 40 min, 2 h, 6 h, and 12 h. (B) Voltage profile of cycles with different cycle time showing the theoretical voltage rise, observed voltage rise, and overpotential in each cycle. (C) Net energy production from each cycle for different cycle time.

voltage rise. The voltage ratio decreased from 98% to 42% (Fig. S7†). Fig. 4C shows the energy production of each cycle. The energy production decreased from 0.12 kW h per m^3 to 0.04 kW h per m^3 (Fig. 4C). When higher currents are applied, overpotentials increase and eventually exceed the voltage rise resulting from the concentration difference between wastewater effluent and seawater. No energy can be recovered. Clearly, this is a condition to be avoided. As noted above, increasing the applied current decreases efficiency and energy production, but high current is needed to give high power output per cell. Furthermore, if the amount of effluent discharged by a wastewater treatment plant is fixed, the number of charges needed to

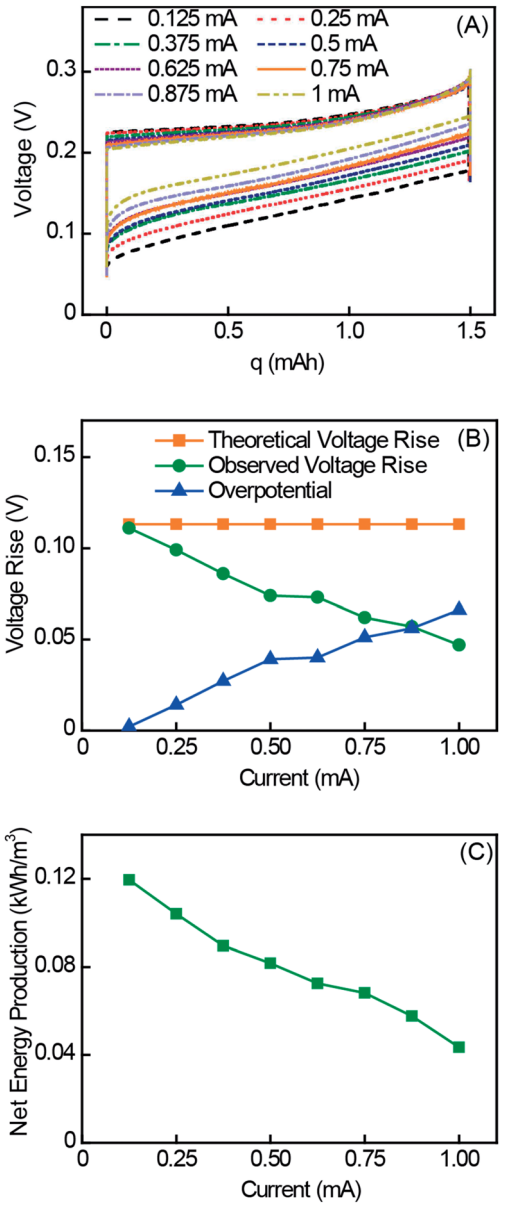

Fig. 4 Cycles at different current with a fixed amount of charge exchanged (1.5 mAh). (A) Energy extraction cycles of mixing entropy batteries at current values ranging from 0.125 mA to 1 mA in a voltage *vs.* charge plot. As current increases, the quadrangle becomes smaller, indicating that less energy is recovered. (B) Voltage profile of cycles at different current showing the theoretical voltage rise, observed voltage rise, and overpotential in each cycle. (C) Net energy production from each cycle at different applied currents.

salinate the effluent remains constant. With the current applied per cell is low, more cells are required, and the capital investment increases. Calculations are needed to determine the optimal trade-off, providing energy efficiency and power output with the minimum capital investment.

Long-term performance of MEBs using Ag/AgCl and NMO electrodes has been tested previously. Performance was stable over 100 cycles.[24] But silver solubility is an issue: in seawater, soluble Ag complexes form with chloride. Because Cl^- concentration could be as high as 0.6 M in seawater, considerable silver can dissolve during cycling. The relevant reactions and equilibrium constants are:

$$AgCl(s) = Ag^+ + Cl^-,\ [Ag^+][Cl^-] = 1.8 \times 10^{-10}$$

$$Ag^+ + Cl^- = AgCl^0,\ \frac{[AgCl^0]}{[Ag^+][Cl^-]} = 10^{3.5}$$

$$Ag^+ + 2Cl^- = AgCl_2^-,\ \frac{[AgCl_2^-]}{[Ag^+][Cl^-]^2} = 10^{5.4}$$

$$Ag^+ + 3Cl^- = AgCl_3^{2-},\ \frac{[AgCl_3^{2-}]}{[Ag^+][Cl^-]^3} = 10^{5.6}$$

$$Ag^+ + 4Cl^- = AgCl_4^{3-},\ \frac{[AgCl_4^{3-}]}{[Ag^+][Cl^-]^4} = 10^{5.2}$$

Neglecting the influence of applied current, the equilibrium concentration of total soluble silver forms is 8.9 ppm, almost 100 times the U.S. EPA secondary drinking water standard of 0.1 ppm.[32] Silver is known to cause adverse health effects including argyria, argyrosis, liver and kidney damage.[33] After 12 hours of cycling, the measured soluble silver concentration in the wastewater effluent was 0.02 ppm and the concentration in the seawater was 0.9 ppm, still an order of magnitude above the EPA standard. Dissolution of silver also increases cost and decreases electrode cycle life. The average loading of the silver electrode is 0.01 g cm^{-2}, giving an estimated cycle life of about 7 years with constantly capacity loss for a Ag/AgCl electrode (based on the measured dissolution of 0.92 ppm Ag in 1.5 mL of solution over a 12 hours cycle). Ag/AgCl electrode was used in this study because its half reaction potential remains stable when oxidized or reduced. However, this analysis indicates that more stable and cheaper anionic electrode materials are needed. Preliminary results show that some conductive polymers will be acceptable as anionic electrode materials in MEBs.

Conclusion

This work establishes that a plate-shape MEB cell can enable a high efficiency of energy recovery from domestic wastewater effluent and seawater. An overall efficiency of 68% was achieved by charging the battery with 12 flushes of recycled wastewater effluent. This demonstrates the potential for recovery of blue energy at coastal wastewater treatment plants. To achieve high net energy recovery efficiencies, cells in series are needed. This results in a trade-off between net energy recovery efficiency and capital investment. We also observe a trade-off between power output and net energy recovery efficiency. These conclusions are independent of the material tested and will be broadly applicable for future optimization efforts where different users may

assign different relative weightings to net energy recovery efficiency, capital investment, and power output. The actual net energy recovery efficiency will also depend upon local conditions, such as requirements for pretreatment and pumping. Finally, this work clarifies electrode material properties that would be desirable for practical application. The ideal MEB electrode materials would enable a rapid potential response to changes in the concentrations of Na^+ and Cl^-; remain stable in wastewater effluent and seawater over many cycles; and be abundant and cheap.

Acknowledgements

Support for this research was provided by the Woods Institute for the Environment at Stanford University and by the U.S. NSF Engineering Research Center Re-inventing the Nation's Urban Water Infrastructure. Support for X. X. was provided by a Stanford Interdisciplinary Graduate Fellowship; support for M. P. was provided by the Oronzio and Niccolò de Nora Foundation.

References

1 P. L. McCarty, J. Bae and J. Kim, *Environ. Sci. Technol.*, 2011, **45**, 7100.
2 E. S. Heidrich, T. P. Curtis and J. Dolfing, *Environ. Sci. Technol.*, 2011, **45**, 827.
3 B. E. Logan and M. Elimelech, *Nature*, 2012, **488**, 313.
4 J. W. Post, *Blue Energy: electricity production from salinity gradients by reverse electrodialysis*, 2009.
5 O. Levenspiel and N. De Nevers, *Science*, 1974, **183**, 157.
6 S. Loeb, *J. Membr. Sci.*, 1976, **1**, 49.
7 S. E. Skilhagen, J. E. Dugstad and R. J. Aaberg, *Desalination*, 2008, **220**, 476.
8 T. Thorsen and T. Holt, *J. Membr. Sci.*, 2009, **335**, 103.
9 R. E. Pattle, *Nature*, 1954, **174**, 660.
10 J. N. Wienstein and F. B. Leitz, *Science*, 1976, **191**, 557.
11 R. E. Lacey, *Ocean Eng.*, 1980, **7**, 1.
12 J. W. Post, H. V. M. Hamelers and C. J. N. Buisman, *Environ. Sci. Technol.*, 2008, **42**, 5785.
13 J. Veerman, M. Saakes, S. J. Metz and G. J. Harmsen, *J. Membr. Sci.*, 2009, **327**, 136.
14 M. Olsson, G. L. Wick and J. D. Isaacs, *Science*, 1979, **206**, 452.
15 W. Finley and E. Pscheidt, US Patent 6,313,545, 2001.
16 D. Brogioli, R. Ziano, R. A. Rica, D. Salerno, O. Kozynchenko, H. V. M. Hamelers and F. Mantegazza, *Energy Environ. Sci.*, 2012, **5**, 9870.
17 R. A. Rica, R. Ziano, D. Salerno, F. Mantegazza, R. V. Roij and D. Brogioli, *Entropy*, 2013, **15**, 1388.
18 M. F. M. Bijmans, O. S. Burheim, M. Bryjak, A. Delgado, P. Hack, F. Mantegazza, S. Tenisson and H. V. M. Hamelers, *Energy Procedia*, 2012, **20**, 108.
19 D. Brogioli, *Phys. Rev. Lett.*, 2009, **103**, 058501.
20 D. Brogioli, R. Zhao and P. M. Biesheuvel, *Energy Environ. Sci.*, 2011, **4**, 772.
21 B. B. Sales, M. Saakes, J. W. Post, C. J. N. Buisman, P. M. Biesheuvel and H. V. M. Hamelers, *Environ. Sci. Technol.*, 2010, **44**, 5661.
22 F. Liu, O. Schaetzel, B. B. Sales, M. Saakes, C. J. N. Buisman and H. V. M. Hamelers, *Energy Environ. Sci.*, 2012, **5**, 8642.
23 M. C. Hatzell, R. D. Cusick and B. E. Logan, *Energy Environ. Sci.*, 2014, **7**, 1159.
24 F. La Mantia, M. Pasta, H. D. Deshazer, B. E. Logan and Y. Cui, *Nano Lett.*, 2011, **11**, 1810.
25 N. Boon and R. Roij, *Mol. Phys.*, 2011, **109**, 1229.
26 Y. Oren, *Desalination*, 2008, **228**, 10.
27 S. Porada, R. Zhao, A. van der Wal, V. Presser and P. M. Biesheuvel, *Prog. Mater. Sci.*, 2013, **58**, 1388.
28 J. B. Lee, K. K. Park, H. M. Eum and C. W. Lee, *Desalination*, 2006, **196**, 125.
29 S. Jeon, H. Park, J. Yeo, S. Yang, C. H. Cho, M. H. Han and D. K. Kim, *Energy Environ. Sci.*, 2013, **6**, 1471.
30 R. Zhao, O. Satpradit, H. H. M. Rijnaarts, P. M. Biesheuvel and A. van der Wal, *Water Res.*, 2013, **47**, 1941.
31 M. Pasta, C. D. Wessells, Y. Cui and F. La Mantia, *Nano Lett.*, 2012, **12**, 839.
32 U. S. EPA, *National Secondary Drinking Water Regulations*, 1979.
33 P. L. Drake and K. J. Hazelwood, *Ann. Occup. Hyg.*, 2005, **49**, 575.

